EXPERIMENTAL APPROACH TO INVESTIGATE THE DYNAMICS OF MIXING COOLANT FLOW IN COMPLEX GEOMETRY USING PIV AND PLIF TECHNIQUES

by

Ezddin HUTLI* *, Valer GOTTLASZ, Daniel TAR, Gyorgy EZSOL, and Gabor BARANYAI

Centre for Energy Research, Thermo-Hydraulics Department, Hungarian Academy of Sciences, Budapest, Hungary

Original scientific paper
DOI: 10.2298/TSCI130603051H

The aim of this work is to investigate experimentally the increase of mixing phenomenon in a coolant flow in order to improve the heat transfer, the economical operation and the structural integrity of light water reactors-pressurized water reactors. Thus the parameters related to the heat transfer process in the system will be investigated. Data from a set of experiments, obtained by using high precision measurement techniques, particle image velocimetry, and planar laser-induced fluorescence are to improve the basic understanding of turbulent mixing phenomenon and to provide data for CFD code validation. The coolant mixing phenomenon in the head part of a fuel assembly which includes spacer grids has been investigated (the fuel simulator has half-length of a VVER 440 reactor fuel). The two-dimensional velocity vector and temperature fields in the area of interest are obtained by both technique. The measurements of the turbulent flow in the regular tube channel around the thermocouple proved that there is rotation and asymmetry in the coolant flow caused by the mixing grid and the geometrical asymmetry of the fuel bundle. Both Results of both techniques showed that at the level of the core exit thermocouple the coolant is homogeneous. The discrepancies that could exist between the outlet average temperature of the coolant and the temperature at in-core thermocouple were clarified. Results of the applied techniques showed that both of them can be used as good provider for data base and to validate CFD results.

Key words: *flow dynamics, mixing phenomenon, temperature distribution, spacer, shear stress, normal stress*

Introduction

The effective parameter to improve the economic attractiveness of light water reactors (LWR) is the power density (*i. e.*, power produced per unit volume of the reactor core). Because the capital cost of a typical LWR constitutes approx. 65% of the total power cost, extracting more energy from an existing reactor or reducing the physical size of future LWR may considerably reduce the total cost of nuclear power. There are various approaches to enhance the power of a LWR. First, through careful management of the fuel assemblies in the core, it is possible to

* Corresponding author; e-mail: ezddinhutli@yahoo.com

flatten the power distribution and thus extract more energy from each assembly on average. Second, using advanced fuel designs and geometries such as annular fuel or non-traditional cladding materials, *e. g*. silicon carbide, it is possible to operate the core at higher power density while maintaining the safety margins [1]. An example of attempts to increase the power production of a LWR-PWR is in Hungary. The cheapest source of energy in Hungary is nuclear power plant (NPP) which encourages the investigations in this field. In order to increase the performance of the existing NPP (LWR-PWR) while keeping to the safety principles, many deep studies have been done, and the conclusion was that the power enhancement can be carried out by the enhancement of the heat performance of the reactor. It must be carried out adhering to the following principles: fixed safety criteria, operation life time of the NPP is not affected, no detrimental effect on failures or maintenance process of unites in NPP, and the service life extension is at least the time of recovering the investment. The feasibility study of capacity upgrade was prepared with about a years' job by centre for energy research (CER). The most important result of the study is that the heat performance of the reactors can be enhanced by 8% while keeping the safety limits. The goal was to enhance the heat performance of the reactor from 1,375 MW to 1,485 MW and to reach at least 500 MW electric performance by this enhancement. Also, it was found that the thermal performance improvements need a new type of fuel assemblies with keeping to safety margin [2]. In order to achieve this goal stricter design is needed. One reason of the performance limit is the conservative calculation of the sub-channel outlet temperature which is not taking into account the mixing process. It is also unknown how the temperature sensors' output values change when the mixing is considered as well.

In the VVER type pressurized water reactors (the subject of the discussion here), the core outlet temperature field is monitored with in-core thermocouples, which are positioned above fuel assemblies. These thermocouples are assumed to be the sources of the essential information about the core situation. For this reason, interpretation of the thermocouple signals is an important task. Originally, under the assumption that perfect coolant mixing existed in the head parts of the fuel assemblies, the measured values were interpreted as the outlet average coolant temperatures of the assemblies. However, for power upgrade point of view, the discrepancies between coolant outlet temperature and that recorded from thermocouples are considered as the essential points in research activities [3]. Many researchers investigated this phenomenon numerically using computational fluid dynamics (CFD) codes and experimentally using fuel assembly simulator (models) and other measurement techniques [3-15]. As the spacer grids (beside their main function as supporters) are assumed to be the main tool in fuel assemblies to increase the mixing phenomenon production rate enhancing the local heat transfer performance in the grid vicinity, this will be associated with increase in pressure drop. Considering these important thermo-hydrodynamic features, the spacer grids are often under improvement to obtain an optimal situation between pressure drop and enhanced heat transfer; many investigations have been done in this subject [3, 5, 6, 9, 11, 15].

This paper deals with an important special aspect of the prediction of the velocity and temperature distribution in reactor core passages of the rod bundle. The basic problem involves what is variously called mixing or turbulent interchange, the “mixing” or “interchange” term represents interactions between the fluid flows in adjacent sub-channels. The purpose of this paper is to define and illustrate the problem, and to gather the data on mixing phenomenon using high technique tools – particle image velocimetry (PIV) and planar laser-induced fluorescence (PLIF), in order to use them to validate the results of CFD, and to find out some patterns for predicting the size of mixing in a given situation. To keep this illustrative approach simple, we assumed that the coolant has a constant density and that no objects stand out into the sub-channels,

that is, the sub-channel cross-sections are uniform with length. The experimental data presented in this paper include explanation of the various cases tested such as test rigs dimensions, measurement zones. The techniques, methodology, test equipment and the boundary conditions were chosen carefully to provide appropriate data for further work with CFD calculations. The obtained data are analyzed in order to highlight the mixing phenomena. Measurement uncertainties are quantified and the error analysis methodology is presented.

Methods and tools

The fuel bundle model (fuel simulator)

The fuel bundle model was built with the use of some original parts and it was inserted in a test rig (PMK), fig. 1. A schematic drawing of the assembly head model and a photograph of the core exit channel can be seen in fig. 2. The test section and the PIV/PLIF system are shown in fig. 3.

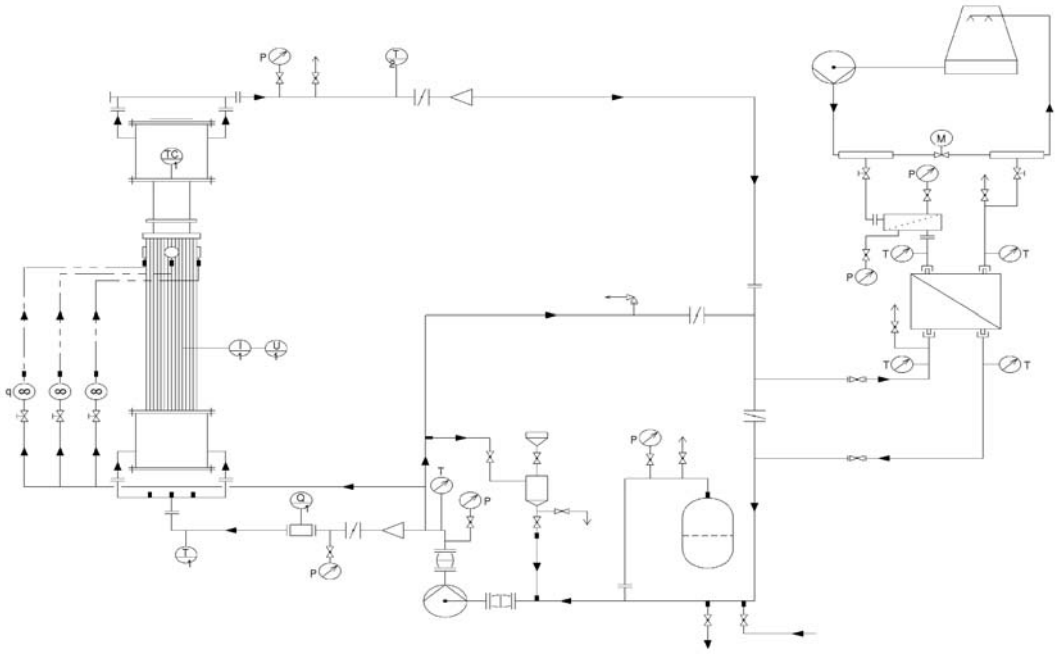

Figure 1. Schematic diagram of the test facility; fuel assembly model and gap flow pipes (on the left), flow rate control system and pump (in the middle) and the cooling loop (on the right)

As in the plant, the fuel rods are surrounded by a hexagonal shroud and at the entrance to the upper head a mixing grid is placed. Downstream of the mixing grid the hexagonal (flow) geometry changes to a cylindrical one. At the following part there are two pins which originally serve for the lifting of the bundle from the reactor core. The upper part following this level comprises the catcher (for fitting the bundles to the core exit channel in the reactor) and the core exit thermocouple. Both have a mixing effect on the coolant flow. The following parts of the model were made of glass and PMMA (PMMA is a transparent thermoplastic, often used as a lightweight or shatter-resistant alternative to glass) in order to be transparent for the laser beam:

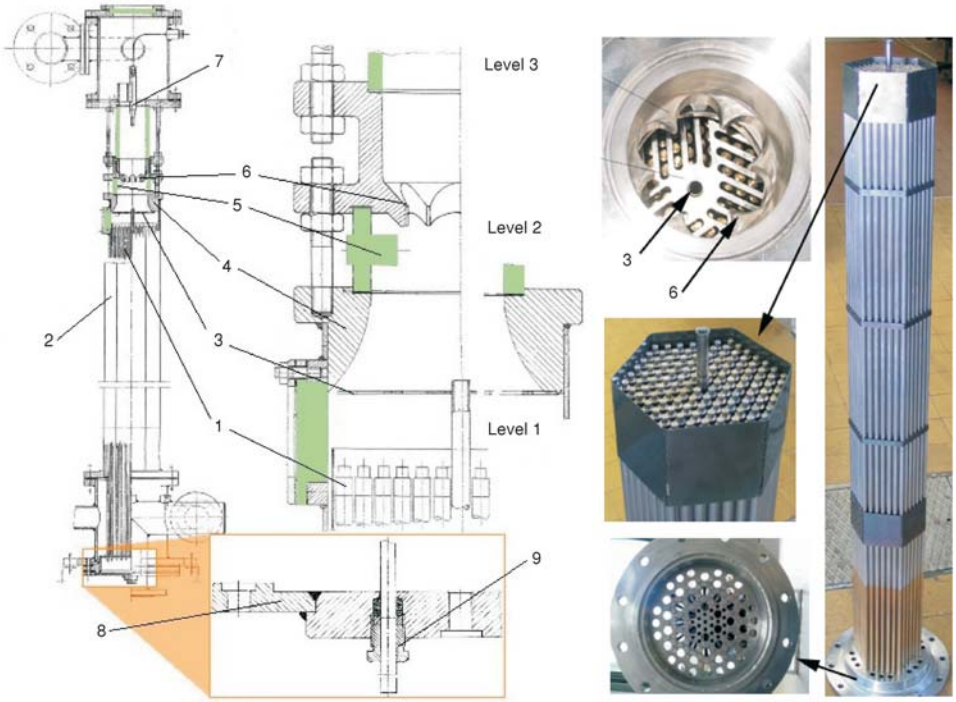

Figure 2. Construction drawing of the fuel bundle model, photograph of the core exit channel and fuel assembly
(1) fuel rods, (2) hexagonal shroud,(3) mixing grid, (4) the hexagonal geometry changes to cylindrical, (5) lifting pins, (6) catcher, (7) in-core thermocouple, (8) bottom plate, (9) fuel rod lead-through stuffing box

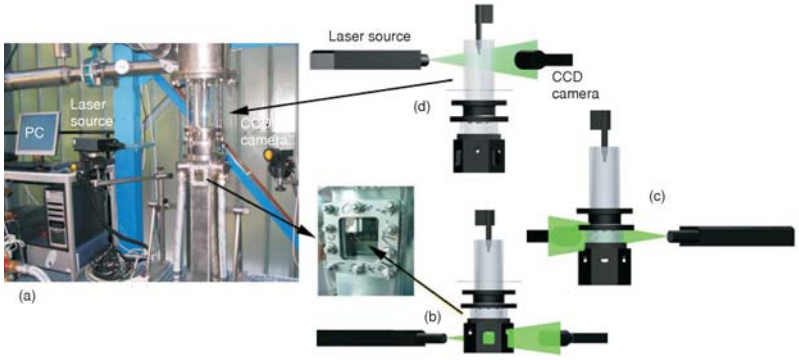

Figure 3. (a) The test section and the PIV/PLIF system, measuring configuration (b) level 1, (c) level 2, (d) level 3

– at the hexagonal part of the fuel bundle three measuring windows were created with a120° symmetry, where the velocity and temperature distribution of the coolant leaving the fuel rods can be measured, level 1, fig.3 (c).
– the 200 mm long tube part comprises the outlet thermocouple; the coolant stream conditions (velocity and temperature distributions) around the thermocouple housing can be investigated here, level 2, fig. 3(b).
– the tube part before the catcher is 40 mm long; it comprises the two lifting pins, which also have an influence on the velocity distribution, and

– the window on the top of the model enables recording the flow distribution in the cross--section area, *i. e*. measuring the velocities in the horizontal plane.

The model (fuel simulator) consists of 126 fuel rods, 36 of them can be heated by cartridge heaters with 72 kW total power, and the heated length is 900 mm. The total length of the rods is 1100 mm, the pitch of rod-to-rod is 12.3 mm. The hexagonal housing containing the rods has cross-section of 160 × 142 mm. A cooling loop takes away the heat of about 30 kW circulation pump. At the PLIF measurements the cooling loop was closed, and the heat of the pump was used for the calibration allowing homogenous temperature distribution.

The applied laser optical techniques (PIV, PLIF)

PIV measurements were done with micro size particles with density near to that of the fluid used, seeding particles dispersed in the fluid and green filter at 532 nm were applied. In PLIF measurements fluorescent dye (Rhodamine B) is dissolved in the fluid flow, and high-pass filter at 550 nm orange is to be applied. In order to have high precision results of PIV measurement, the scaling factor calibration has been applied for the determination of the absolute velocities, while in case of PLIF measurement the intensity-temperature calibration for each pixel is essential. Calibration was done using the circulation pump power input. In PIV measurements, the diameter of the polyamide seeding particles was 20 m and their density was 1.016 g/cm^3, which was equal to the water density. Therefore, the velocity of the particles represents the velocity of the coolant. The typical investigation area size was 16×16 pixel, and cross correlation was used for the calculation. The time between the two laser impulses was set to 100 s. The time averaged velocity field results have been obtained by recording 500-1000 frame pairs at 2-4 Hz frequency. The energy of the Nd YAG laser was set to 20% of the maximum 50 mJ.

The PLIF measurement technique is designed to determine a temperature field in a planar cross section of a flow field. The Rhodamine B was excited by the same laser that was used for PIV measurements. The intensity of the local fluorescent light depends on the Rhodamine concentration, the exciting laser power and the temperature of the water. Therefore it is necessary to keep all these parameters fixed. The calibration of the LIF data is necessary before each measurement. The inhomogeneity of the laser beam has been eliminated by doing the calibration for each pixel individually. At the PLIF measurements the cooling loop was closed, and the heat of the pump was used for the calibration ensuring homogenous temperature distribution. The LIF images contain mean pixel values of a few hundred successive images.

Measurement set-up and conditions

Measurements were carried out at three axial levels of the fuel channel. Level 1 is just above the top of fuel rods; its lower boundary is the outlet of the subchannels, its upper boundary is the mixing grid. Level 2 is the tube part before the catcher; it comprises the two lifting pins which also have an influence on the velocity distribution. Level 3 is around the central thermocouple; it is the most important region related to the study of coolant mixing. Several heating configurations were set for the experiments, some of them have been chosen to be presented here. The fuel rods (of the fuel simulator) were numbered according to the convention used in reactor physics and thermal hydraulics. In the case of "A" (total) configuration, fig. 4(a), all the possibly heatable rods are switched on (72 kW); the distribution of the 36 heatable rods is symmetric; each second neighbor is heatable, in the "C" case, fig. 4(c), the marginal rods are heated (36 kW). In order to investigate the influence of coolant flow rate on the mixing phenomenon in the fuel rods, five flow rates were employed in this work (10, 30, 50, 70, and 90 m^3/h), the maximum inlet pressure was 3 bar, and maximum temperature was 80 °C (both values of the pressure

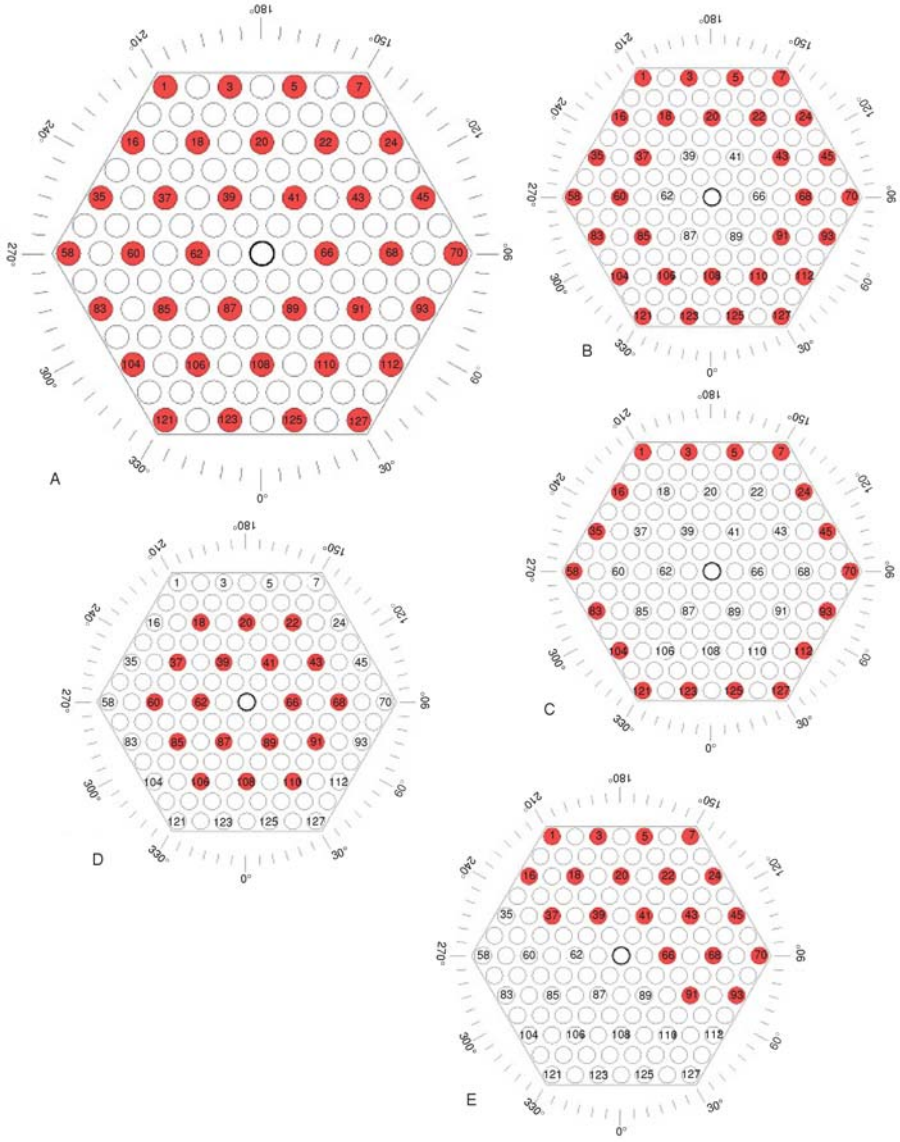

Figure 4. A, B, C, D, and E "Model" heating configuration (A "Model" is enlarged)

and of the temperature are far from real values in the reactor), the PIV and PLIF measurements were done with these flow rates under different heating power, heat configuration, and different position of measurements. Not all results will be presented for lack of space and to avoid repetition.

Measurement results and discussion

The obtained results of PIV presented in figs. 5, 6, 7, and 8, respectively, are related to the measurements done at a specified level of the three levels presented in figs. 2 and 3.

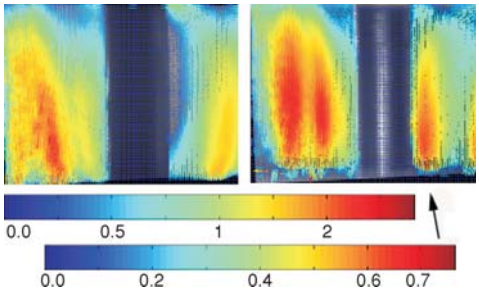

Figure 5. PIV velocity distributions, [ms^{-1}] level 1 Q = 30 and 90 m^3/h
(for color image see journal we site)

Figure 5 shows the time averaged velocity field between the top of the fuel rods and the mixing grid which place is named level 1. The scaling factor for the absolute velocity values was calibrated to the central tube of 10.3 mm diameter. In this case the laser beam and the axis of the camera were not at 90°, but at an angle of 120°. As a result, the images recorded are distorted due to the perspective. They were corrected with an imaging model fit (camera calibration) compensating the distortion (Dantec, 2000). The laser sheet is 7 mm behind the center pipe to avoid too much disturbing light towards the camera reflected by center pipe surface. So there is a blind spot on the pictures covered by the centre pipe. The scale factor was based on the diameter of the center pipe. Figure 5 shows the velocity distributions at two flow rates Q = 30 m^3/h and Q = 90 m^3/h, respectively, the influence of the sub-channels resulting plumes of the higher velocities. Higher velocity plumes can be observed at the lower part of the image, at the fuel subchannel outlets. Regarding the upper part of the image, the effect of the mixing grid to the flow field can be clearly discovered, as the measured area extended to the mixing grid. At a lower flow rate (Q = 30 m^3/h) the plume lengths and shapes are less regular in consequence of the lower impulse of the flow. In addition the maximum velocity achieved depends on the flow rate. The lengths of the velocity vectors in this field at 30 m^3/h were between 0.2 and 0.75 m/s while at 90 m^3/h flow rates were between 0.5 and 3.5 m/s.

Figure 6 shows the obtained results of PIV at level 2 for two flow rates Q = 30 m^3/h and Q = 90 m^3/h, respectively. For measurements in level 2 the laser beam and the axis of the camera were at 90°. In fig. 6 the time averaged velocity field in the area below the catcher can be seen (level 2). In this part there are two pins which appeared as black borders in the right part of fig. 6(b), which in the real fuel bundle serve for the lifting of the assemblies. In the model they were made of PMMA as parts of the cylindrical tube. For absolute velocity calibration a ruler was placed to the measurement plane. The lengths of the velocity vectors in this field at 30 m^3/h were

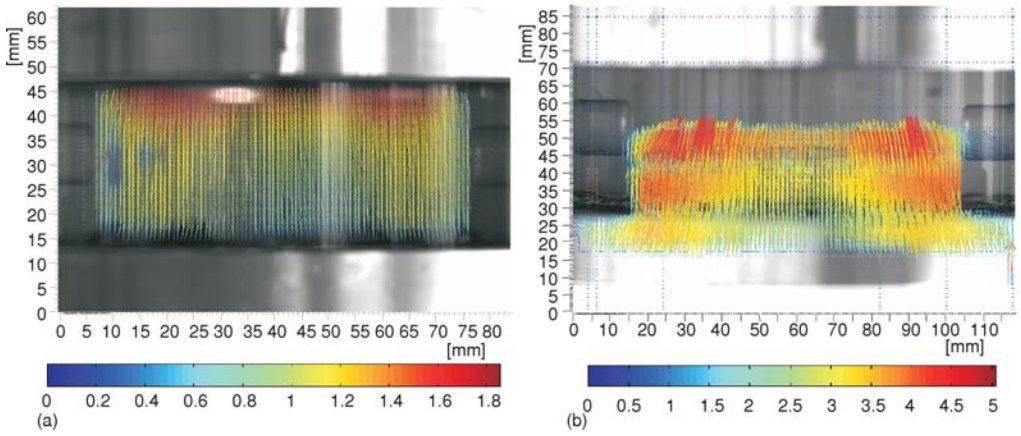

Figure 6. PIV velocity distributions [ms^{-1}], level 2, Q =30 and 90 m^3/h
(for color image see journal we site)

between 0.8 and 1.8 m/s while at 90 m^3/h flow rates were between 2 and 4.5 m/s, in the vicinity of the catcher some higher velocity plumes were observed, exceeding 1.9 and 5 m/s for flow rates 30 m^3/h and 90 m^3/h, respectively. This proved to be the highest velocity regarding the flow field of the whole model. The influence of the mixing grid on the flow field can be also clearly discovered around the tube centerline. Around the central part of the mixing grid there is no path for the flow; it changes the upstream flow distribution, causing a low velocity region in the middle of the channel, this is clearer seen in case of flow rate 30 m^3/h.

Level 3 in the test section was determined for the measurements of the cylindrical tube part (core exit channel as in figs. 2 and 3) – at this level the angle between the laser beam and the axis of the camera was 90°, the scaling factor for the absolute velocities was calibrated to the 8.5 mm diameter tube part of the thermocouple, which appears on the particle image recordings of flow rate 30 m^3/h. The vertical components of the maximum velocities are around 1.8 m/s at

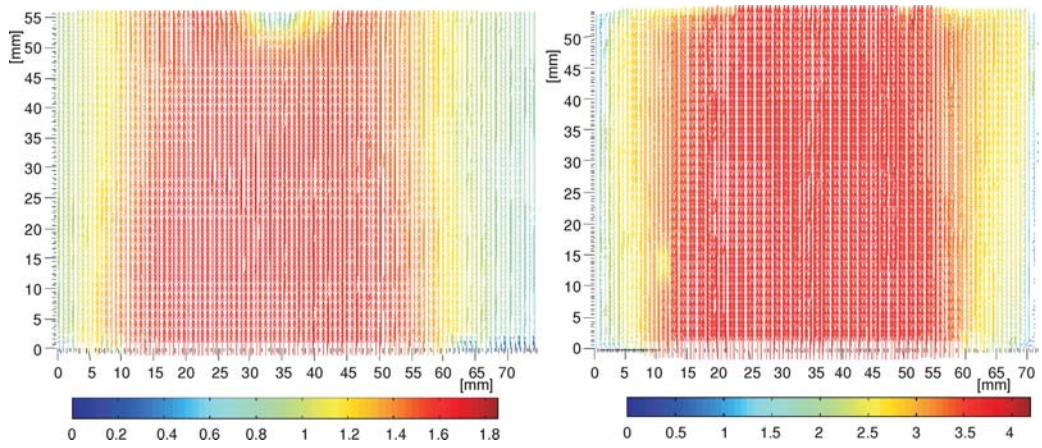

Figure 7. Average PIV velocity distribution [ms^{-1}], level 2, Q = 30 and 90 m^3/h
(for color image see journal we site)

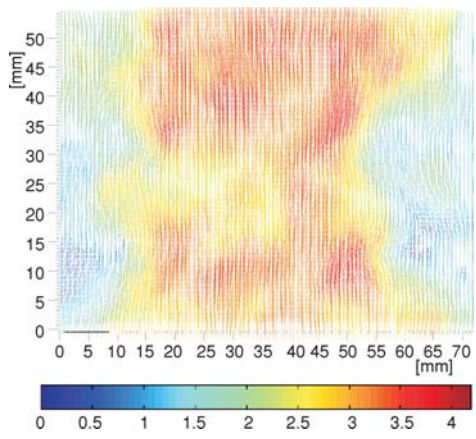

Figure 8. Instantaneous PIV velocity distribution [ms^{-1}], level 2, Q = 30 m^3/h
(for color image see journal we site)

flow rate 30 m^3/h and around 4 m/s at flow rate 90 m^3/h. The local influence of the thermometer on the time averaged velocity field can be clearly discovered (fig. 7, left side). On the time averaged vector map for both flow rates 30 and 90 m^3/h at the lower part of the tube a low velocity region can be observed at the sides, which is getting narrower in the upper region; this is due the influence of the catcher. An instantaneous velocity vector map measured at the lower region is shown in fig. 8. The instantaneous distribution displays the fluctuations of the turbulent flow on the vector map vortexes and plumes can be seen which disappear in the time averaged case. The chaotic instantaneous distribution is the consequence of the flow mixing effect of the mixing grid and the catcher.

Figures 9, 10, and 11 show the temperature distribution as result of three heating configurations (A, B, and C "Model") as presented in fig. 3, respectively. The results are related to the measurements done at level 1; they show that at a low flow rate (Q = 10 m^3/h) the temperature distribution indicates the higher temperature of the coolant in the sub-channels; with increase of the flow rate (Q = 30 m^3/h) the effect of the mixing grid is also observable. In addition the temperature map depends on the heating configuration model.

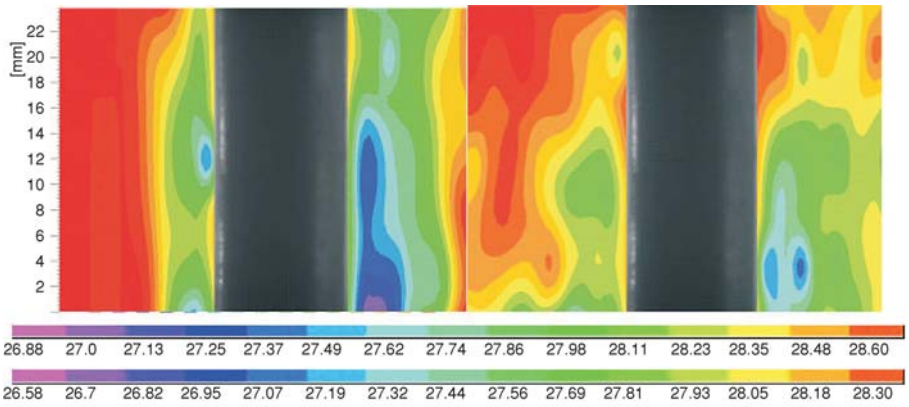

Figure 9. PLIF temperature distributions, level 1, "A-Model" heating configuration [°C], Q = 10 and 30 m^3/h, respectively (for color image see journal we site)

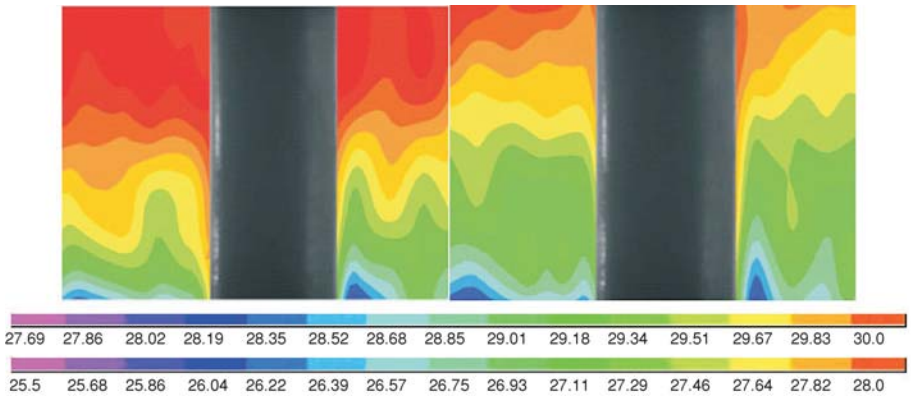

Figure 10. PLIF temperature distributions, level 1, "B-Model" heating configuration [°C], Q = 10 and 30 m^3/h, respectively (for color image see journal we site)

The comparison between the results shows that in fig. 6 the effect of subchannels on the temperature distribution is clearer than that in the other two figs. (7 and 8), this is because the measurement window is too small and the effect could be seen out of this range.

In figs. 7 and 8 as a result of existing the mixing grid which is right above this interrogation region the hot water was collected closer to the center pipe. On the bottom of the pictures, the effect of the subchannels still can be seen. Further measurements are needed for the correct

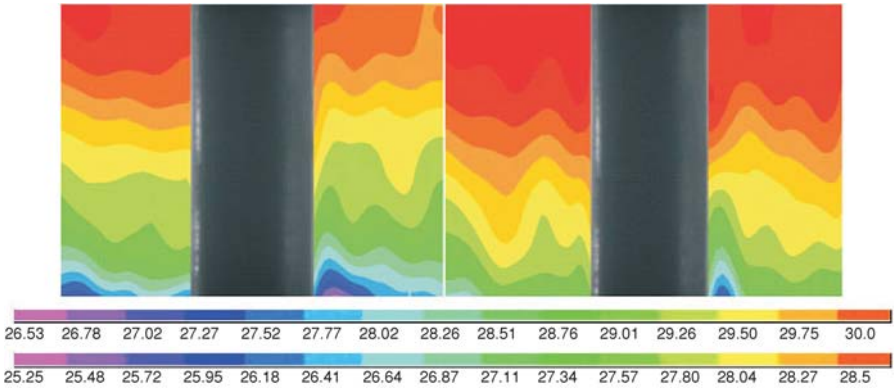

Figure 11. PLIF temperature distributions, level 1, "C-Model" heating configuration [°C], Q = 10 and 30 m^3/h, respectively (for color image see journal we site)

explanation of the temperature. From results shown in fig. 6, the difference between maps of the temperature distribution was not such as expected considering to the big difference between applied flow rates. At Q = 30 m^3/h, where the upper region is nearly as warm as at Q = 10 m^3/h, a good example is shown in fig. 10. The effect could be the consequence of an inaccuracy of the PLIF measurements.

Figures 12 and 13 show the PLIF results at level 2 for B and C heating models, respectively. The analysis of the PLIF images revealed that for both models of heating configuration

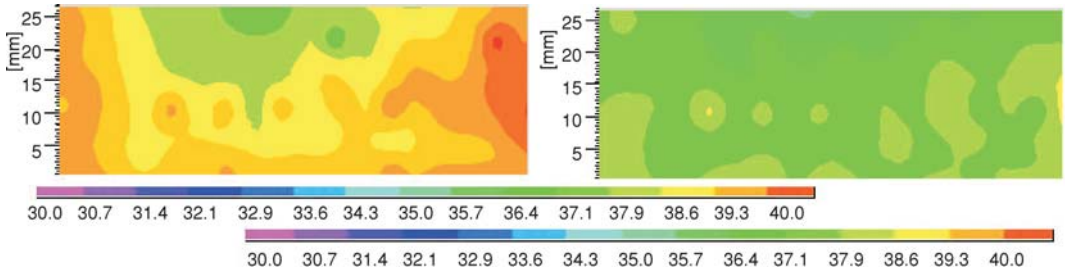

Figure 12. PLIF temperature distributions, level 2, "B-Model" heating configuration [°C], Q = 10 and 30 m^3/h, respectively (for color image see journal we site)

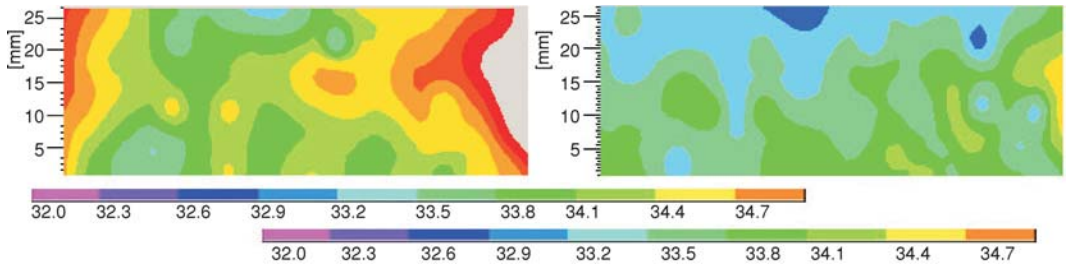

Figure 13. PLIF temperature distributions, level 2, "C-Model" heating configuration [°C], Q = 10 and 30 m^3/h, respectively (for color image see journal we site)

there are higher temperatures near vertical edges and some plumes of relatively higher temperature appeared. At 30 m^3/h there are lower temperatures because of the higher velocity and larger mass flow leading to less warming fluid. The deviation between temperature degrees recorded in fig. 12 and in fig. 13 is a result of different heating models.

Figures 14 and 15 represent the obtained results of the measurements at level 3 (cylindrical core exit channel) for C and D heating model, respectively. The analysis of results in fig. 14 show that there is no measurable influence of the sub-channels, at this level the higher velocity and higher temperature plumes disappear even at inhomogeneous heating configuration and low flow rate, mainly as a consequence of the mixing grid.

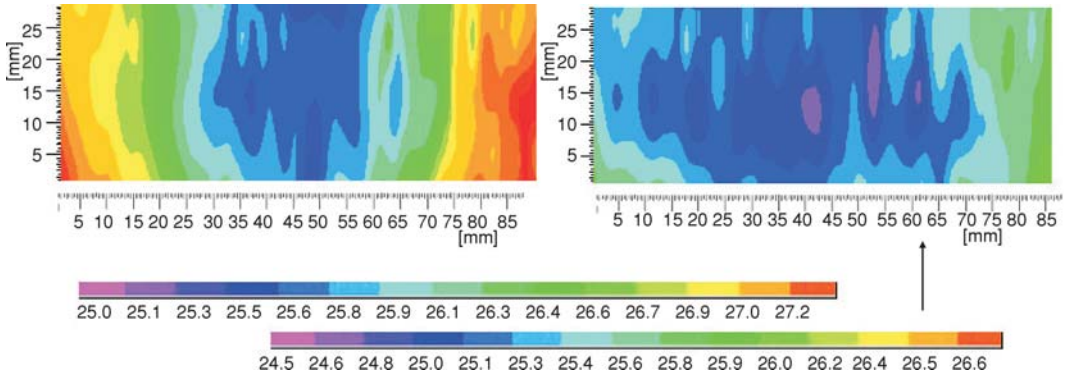

Figure 14. PLIF temperature distributions, level 3, "C-Model" heating configuration, [°C], Q = 10 and 30 m^3/h (for color image see journal we site)

The temperature distributions at level 2 were also homogeneous apart from some very inhomogeneous heating configurations, *e. g*. the model "E-Model" as presented in fig. 4(E) and low flow rate. The results related to the inhomogeneous heating are not presented here because of the lack of space. The result of the extreme "C" model heating configuration at 10 and 30 m^3/h is shown in fig. 14. The distribution is symmetric around the image center. In figs. 14 and 15 the vertical dimension differs from the described scalar maps; the PIV region is 55 mm high (figs. 7 and 8), the PLIF map is 30 mm high; the top of the PLIF map is 25 mm under the thermocouple. In general, the average of the absolute values of the temperature is quite near to the temperature measured by the thermometer.

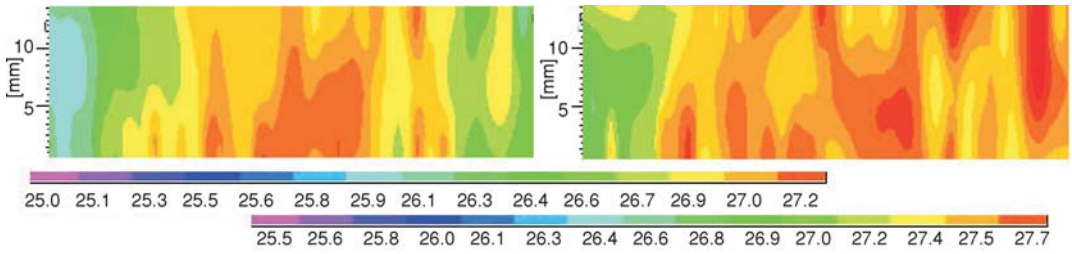

Figure 15. PLIF temperature distributions, level 3, "D-Model" heating configuration, [°C], Q = 10 and 30 m^3/h (for color image see journal we site)

As shown in fig. 16(a), the time averaged velocity profiles are similar at each flow rates, and the profiles are symmetric, just like the time averaged stress terms, fig. 16(b); this refers to the elements intruding to the flow (mixing grid, lifting pins, catcher) causing turbulent mixing. In fig. 16(a) we can see also that, the standard deviations are high at the borders compared with those in flat regions in each profile and also the standard deviations depend on the flow rate (Reynolds number is changing with geometry path). Standard deviation could be a good indicator for the velocity fluctuation intensity, *i. e*. turbulent intensity. The profiles presented in fig. 16(a) give a simple and efficient way to compare the averaged behavior of the flow at various measured positions and under different flow rate conditions. The PIV velocity measurements showed that at the core exit thermocouple level the velocity distribution of the coolant is homogenized by the mixing grid, lifting pins and the catcher (the plumes disappeared, velocity profiles were cylindrical).

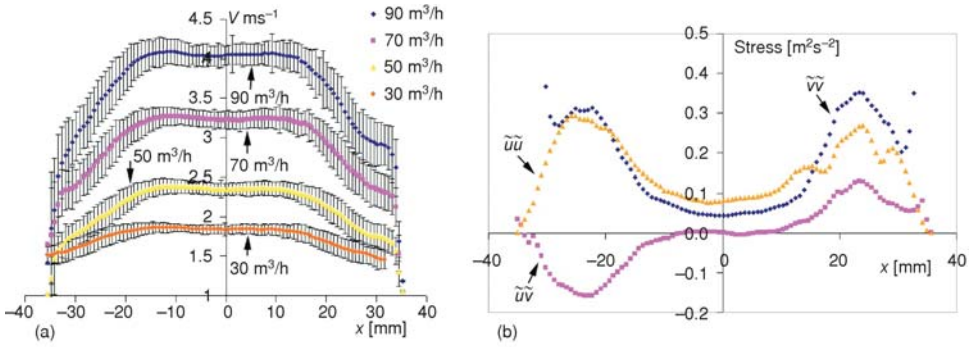

Figure 16. (a) Vertical velocity magnitude and standard deviation, level 2, [ms^{-1}], (b) PIV, time averaged stress terms measured in horizontal profiles, level 2, [ms^{-1}], $Q = 90$ m^3/h (for color image see journal we site)

The turbulent flow regime generally shows a rapid mixing and exchanging of fluid volume across the flow cross-section, the resulting velocity profile is relatively uniform [16]. This interaction between layers of fluid will enhance the extracted heat from the exposed surface but in the meantime the pressure drop will increase, in addition, the fuel rods vibration will increase. As well known, in turbulent flow it is very difficult to define exactly the flow features, especially in such complex geometry. In fuel assembly, the difficulty increases by existence of spacer grids. Grids increase the chaotic motion level. Nevertheless, there are several important characteristics that all turbulent flows possess. These characteristics include unpredictability, rapid diffusivity, high levels of fluctuating vorticity and dissipation of kinetic energy [17]. The additional mixing phenomenon could be a result of the cross-flows induced by geometrical details like spacer grids and by secondary flows induced by the non-circular shape of the flow channel (flow shape change). Also, there is a possibility of time-dependent flow pulsations in gaps between fuel rods that can work as an additional mixing mechanism [18]. The presence of ribs (in our case they are spacers) will promote the convection heat transfer due to increase of the turbulent mixing [19]. In general, as a result of turbulent flow and formation of boundary layers the fluid will suffer from two kinds of stresses: normal and shear stress. In other words, the portions of fluid move irregularly causing a continuous exchange of momentum (momentum is mass multiplied by velocity) from one portion of the fluid to another. This momentum exchange is the reason for the turbulent shear stress. Prandtl's mixing length theory is based on the as-

sumption that a fluid parcel has to travel over a length l m before its momentum is transferred. Basically, for single phase flow, it is easy to understand the concept of the mixing length: since turbulent stress is caused by momentum transfer, it is useful to have a physical length that defines the time when the momentum has been transferred [20]. But here the existence of ribs will lead to transfer the momentum very fast and in less traveling distance. The turbulence intensities (normal stress) and Reynolds stress (shear stress) were calculated using velocity vector fields obtained from PIV measurements; eqs. (1) and (2) are used, respectively. The intensity of turbulence is defined as the RMS value of the fluctuating velocities. The stream-wise (u') turbulent intensities were calculated using eq. (1) and normal (v') turbulent intensities it can be calculated by the same manner using $v'(x, y)$ instead of $u'(x, y)$ in eq. (1). The turbulence intensities in the stream-wise direction, $u'(x, y)$, and normal direction, $v'(x, y)$ of the velocity vector, both of them assumed as normal stress, are presented in fig. 16(b) associated with Reynolds stress which is a shear stress. The stresses are higher near the walls and values are lower at the center of the channel because boundary layer is developed near the walls.

$$u'(x, y) = \sqrt{\frac{\sum_{i=1}^{N}[(u_i(x, y) - U(x, y)]^2}{N}} \tag{1}$$

$$\overline{u'v'} = \frac{1}{N}\sum_{i=1}^{N}[u'(x, y)][v'(x, y)] \tag{2}$$

PIV/PLIF uncertainty investigation

A general discussion of the accuracy of the PIV/PLIF system can be found in [21]. For the system used here, three main steps have been applied for the post-processing of the measured PIV data, validation, time averaging, and space averaging. PIV is an instantaneous measurement technique; all spatial information is sampled at the same time so there will be some regions where there is really no meaningful input and incorrect vectors can occur [22]. In the case of our reported results, peak height and velocity range validation have been carried out. Peak height validation accepts or rejects individual vectors based on the values of the peak heights in the correlation plane where the vector displacement has been measured. Velocity range validation excludes vectors which are outside a certain range [22]. The next step of the post-processing has been the time averaging of the set of our acquired data. The time averaging has been realized by calculating mean velocity vector maps. The standard deviations for each velocity components have also been calculated; they are shown in fig. 17 as the uncertainties of the velocity profiles.

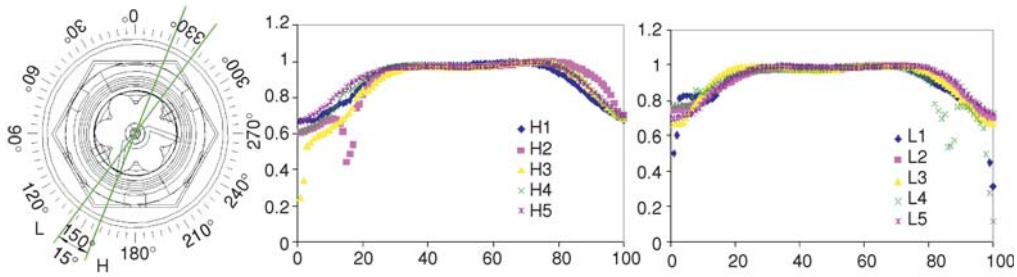

Figure 17. (a) Setup of the PIV repetition test (relative dimensions and velocities), (b) Result of the "L" position of the repetition test, (c) Result of the "H" position of the repetition test
(for color image see journal web site)

According to the diagrams, the magnitude of the vertical velocity fluctuations is lower around the center line of the tube and higher at the sides at all of the tested flow rates.

The final step of post-processing is the filtering of vector maps by arithmetic averaging over vector neighbors. Inside the averaging area the individual vectors are smoothed out by the average vector.

As in this study the results are qualitatively interpreted and visualized, no overall uncertainty analysis was made. However, the error range of the velocity magnitudes can be well approximated by measuring the flow rate at a well known cross-section of the loop – practically it was mounted into a transparent plastic tube which could be illuminated by the laser sheet. In this way the averages of the measured velocities could be compared. The relative uncertainty maximum proved to be about 5%. This can be assigned to the limitations of measuring the 2-D projection of the particle velocities in the flow field. This uncertainty includes the systematic error which comes from measuring the scaling factors.

The vibration of the hydraulic loop cannot be avoided due to the relatively high flow velocities. The vibration is detectable on the particle images. By choosing correctly the investigation areas, the effect of the vibration can be corrected on the time averaged vector maps. In the case of the measurements the Δt (time between the two laser impulses, resulting in two particle images) was set to 100 μs, and the frequency of recording image pairs (vector maps) was 4 Hz. It is possible to check a set of image pairs, mark a fix point of the tube (for example its side) on the image, and notice whether the displacement of the fix point caused by the vibration is smaller or bigger than the size of the investigation area. By choosing the investigation area size big enough, the displacement will not exceed its size. The result vector produced by one particle image pair can be interpreted as a spatial average within one investigation area. By calculating the time averaged vector maps, the vectors belonging to the same investigation area are averaged in time.

The relative uncertainty of the induction flow meter installed in the main line of the loop with the range of 6.4-160 m^3/h was <1.5% within the applied 50-90 m^3/h range. Out of this range ±0.5% can be assigned to the conversion of the flow velocity to electric signal.

Also, a repetition test of the PIV measurements has been done here. Two different adjustments of the system were set – "L" and "H" positions, see fig. 17(a) – then measured alternately, according to L1 → H1 → L2 → H2 → L3 → H3 → L4 → H4 → L5 → H5. It is important to know, that the system was completely switched off and restarted after each measurement. The result diagrams, fig. 17 (b, c) show very good agreement at the central regions of the profiles where the standard deviation is less than 5%; at the sides the uncertainty is somewhat higher. Each measured point is the time average result of 1000 instantaneous measurements.

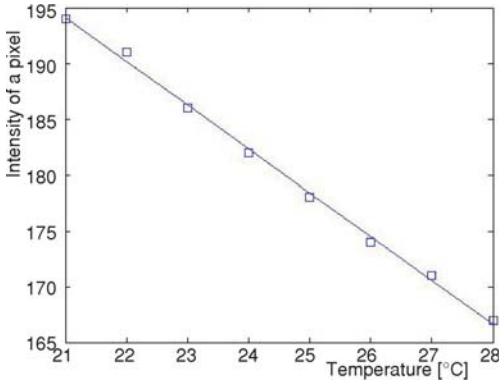

Figure 18. LIF calibration line at the third axial position (level 3)

It is mentioned in the literature that the discrepancies could be due to the integrated effects of many complex flow phenomena such as wake-wake, wake-vane and vane-boundary layer interactions occurring simultaneously in a complex flow environment [23]. It means that high value of accuracy will not be established in these kinds of measurements, thus the repetition of both calibration process and measurements (average to be used) are necessary to get results with high accuracy.

As well known, the accuracy of the LIF basically depends on the quality of calibration process. Before starting with different models of heating configurations, the calibration was made and the accuracy of the thermometers at the inlet and the outlet of the test rig (fuel model) was used as a reference which is ±0.15 °C of full scale. Figure 18 shows a calibration line which was taken at the 3rd axial position. The calibration curve (line) gives reasonable information about the thermal resolution of the measurements. It is a typical calibration line of all the pixels at each position because there were the same conditions and arrangements for all the axial positions. According to this line we can assume that the maximum resolution of the temperature is 0.2 ºC as the intensity of a pixel can change between 1 to 255 (8 bit) but considering the total temperature field we have to consider all the 2 million pixels of a picture. All temperature fields were taken from the average of 180 images by 4 Hz. The measurements performed at the third axial position (level 3) where the reference thermometer is placed, show that the accuracy of the temperature evolved of the calibration is ±0.15 °C.

Conclusions

An experimental investigation was performed successfully with PIV and PLIF techniques to obtain detailed information on the velocity, turbulence and temperature distribution for parallel turbulent flows through sub-channels of rod bundle, this leads to understand the coolant flow mixing process in the head part of a fuel assembly. Qualitative and quantitative analyses of the velocity and temperature distribution in the core exit channel model have been done. The PIV velocity measurement showed that at the level of the core exit thermocouple the coolant is homogenized by the mixing grid, catcher and the lifting pins; the velocity plumes present just downstream of the fuel assembly outlet disappear at the cylindrical tube part of the assembly head. This was proven also by the velocity and the temperature measurements; a strongly asymmetric heating configuration was required to detect significant differences in the temperature distributions at the thermocouple level, in other cases it was nearly homogeneous. Repetition has been done for calibration process and measurements in order to minimize the influence of test rig vibration on the results. The PIV/PLIF measurements technologies proved to be suitable for the investigation of turbulent mixing in the complicated system geometry, Results of the applied these techniques showed that both of them can be used as good provider for data base and to validate CFD results.

References

[1] Jacopo, B., Lin, WH., Nano-Fluid Heat Transfer Enhancement For Nuclear Reactor Applications, *Proceedings*, ASME, 2nd Micro/Nanoscale Heat & Mass Transfer International Conference, Shanghai, China, 2009
[2] Larisza, Sz., Capacity Upgrade at Paks Nuclear Power Plant, http://paksnuclearpowerplant.com/download/1271/FW_%20TNcikk2_n.pdf
[3] Bezrukov, Yu. A., *et al*., Investigation of the Mixing of Coolant Flows in a VVER Vessel, *Atomic Energy, 96* (2004), 6, pp. 391 -398
[4] Rehme, K., Pressure Drop Correlations for Fuel Element Spacers, *Nuclear Technology, 17* (1973), 1, pp. 15-23
[5] Chun, T. H., Oh, D. S., A Pressure Drop Model for Spacer Grids with and without Flow Mixing Vanes, *Journal of Nuclear Science and Technology, 35* (1998), 7, pp. 508-510
[6] Shen, Y. F., *et al*., An Investigation of Cross Flow Mixing Effect Caused by Grid Spacer with Mixing Blates in a Rod Bundle, *Nuclear Engineering and Design, 125* (1991), 2, pp. 111-119
[7] Holloway, M. V., *et al.*, The Effect of Support Grid Features on Local, Single-Phase Heat Transfer Measurements in Rod Bundles, *Journal of Heat Transfer, 126* (2004), 1, pp. 43-53

[8] Kobzarv, L. L. , Oleksyuk D.A., Experiments on Simulation of Coolant Mixing in Fuel Assembly Head and Core Exit Channel of VVER-440 Reactor, 16th Symposium of AER on VVER Reactor Physics and Reactor Safety, Bratislava, Slovac Republic, 2006
[9] Karoutas, Z., *et al.*, 3D Flow Analyses for Design of Nuclear Fuel Spacer, *Proceedings,* 7th International Meeting on Nuclear Reactor Thermal-Hydraulics NURETH-7, New York, USA, 1995, pp. 3153-3174
[10] Imaizumi, M., *et al*., Development of CFD Method to Evaluate 3D Flow Characteristics for PWR Fuel Assembly, Transactions of the 13th International Conference on Structural Mechanics in Reactor Technology SMIRT 13, Porto Alegre, Brazil, 1995, pp. 3-14
[11] Ikeda, K., Hoshi, M., Development of Mitsubishi High Thermal Performance Grid, *JSME International Journal, series B, 45* (2002), 3, pp. 586-591
[12] Ikeno, T., Kajishima, T., Decay of Swirling Turbulent Flow in Rod-Bundle, *Journal of Fluid Science and Technology, 1* (2006), 1, pp. 36-47
[13] Caraghiaur, D., Anglart, H., Measurements and CFD Predictions of Velocity, Turbulence Intensity and Pressure Development in BWR Fuel Rod Assembly with Spacers, *Proceedings*, 12th International Meeting on Nuclear Reactor Thermal Hydraulics (NURETH12), Pittsburgh, Penn., USA, 2007
[14] Sandor, T., Attila, A., CFD Study on Coolant Mixing in VVER-440 Fuel Assembly Head, *Proceedings*, ICAPP '08, Anaheim, Cal., USA, 2008, pp. 1813-1823
[15] Shakir, H., *et al*., CNPP Fuel Rod Vibration Analysis Using Finite Element Method, *Technical Journal*, University of Engineering and Technology Taxila, Special issue onVibration Analysis (2012), pp. 24-34
[16] Gerard, C., *et al*., Fluid flow Fundamentals, *Oilfield Review Winter 1996, Schlumberger*, Vol. 8 issue 4, pp. 61-64
[17] Philip, J. W., Donald, R. W., Turbulent Diffusion, School of Civil and Environmental Engineering, Georgia Institute of Technology, Atlanta, Geo., USA, pp. 1-42 http://itia.ntua.gr/~panospap/DPMS_PERIBALLONTIKH%20YDRAULIKH/Other_Material/Roberts_Turb_Diffusion.pdf
[18] Toppila, T., Lestinen, V., CFD Simulation of Coolant Mixing Inside the Fuel Assembly Top Nozzle and Core Exit Channel of a VVER-440 Reactor, *Proceedings*, 14th Symposium of AER on VVER Reactor Physics and Reactor Safety, Espoo, Finland & Baltic Sea Cruise to Stockholm, 2004
[19] Mushatet, K. S., Simulation of Turbulent Flow and Heat Transfer over a Backward Facing Step with Ribs Turbulators, *Thermal Science, 15* (2011), 1, pp. 245-255
[20] Agrawal, A., Prasad, A., Measurements within Vortex Cores in a Turbulent Jet, *Journal of Fluids Engineering, Transaction of the ASME, 125* (2003), 3, pp. 561-568
[21] Raffel, M., *et al*., Particle Image Velocimetry: a Practical Guide Berlin Heidelberg New York, Springer 978-3-54072307-3, 2007
[22] Dantec Dynamics, FlowManager Software and Introduction to PIV Instrumentation Software User´s guide, Dantec Dynamics A/S, 2000
[23] Elvis, E. D., *et al*., Experimental Benchmark Data for PWR Rod Bundle with Spacer-Grids, *Proceedings*, CFD for Nuclear Reactor Safety Applications (CFD4NRS-3) Workshop, Bethesda, Md., USA, 2010

Paper submitted: June 3, 2013
Paper revised: February 26, 2014
Paper accepted: March 27, 2014